Strong decays of T_{cc}^+ at NLO in an effective field theory

Lin Dai,[1,*] Sean Fleming,[2,†] Reed Hodges,[3,‡] and Thomas Mehen[3,§]

[1]Physik Department, Technische Universität München, 85748 Garching, Germany
[2]Department of Physics and Astronomy, University of Arizona, Tucson, Arizona 85721, USA
[3]Department of Physics, Duke University, Durham, North Carolina 27708, USA

(Received 14 February 2023; accepted 11 March 2023; published 3 April 2023)

The T_{cc}^+ exotic meson, discovered by the LHCb Collaboration in 2021, can be interpreted as a molecular state of $D^{(*)0}$ and $D^{(*)+}$ mesons. We compute next-to-leading-order (NLO) contributions to the strong decay of T_{cc}^+ in an effective field theory for D mesons and pions, considering contributions from one-pion exchange and final-state rescattering. Corrections to the total width, as well as the differential distribution in the invariant mass of the final-state D-meson pair are computed. The results remain in good agreement with LHCb experimental results when the NLO contributions are added. The leading uncertainties in the calculation come from terms which depend on the scattering length and effective range in D-meson scattering.

DOI: 10.1103/PhysRevD.107.076001

I. INTRODUCTION

The LHCb Collaboration has observed a narrow resonance, the exotic tetraquark T_{cc}^+, in the final state $D^0D^0\pi^+$ [1–5]. The resonance is close to both the $D^{*0}D^+$ and $D^{*+}D^0$ thresholds. When using a unitarized Breit-Wigner profile appropriate for a coupled-channel problem, LHCb finds the difference between the resonance mass and the $D^{*+}D^0$ threshold, δm, and the decay width, Γ, to be [5]

$$\delta m = -360 \pm 40^{+4}_{-0}\ \text{keV},$$
$$\Gamma = 48 \pm 2^{+0}_{-14}\ \text{keV}. \tag{1}$$

The $D^{*0}D^+$ threshold is 1.7 MeV above the resonance. The closeness of the resonance to the two thresholds suggests the possibility that T_{cc}^+ has a molecular nature.

After the announcement of the discovery of T_{cc}^+, many theory papers attempted to understand various aspects of the exotic meson [6–26]. Several papers tried to predict its decay width and differential decay width, with considerable success [6,7,10,13,14,20,21]. In one of these papers [6], we wrote down an effective field theory for T_{cc}^+, considering it a molecular state of two D mesons treated nonrelativistically, and computed leading-order strong and electromagnetic decays. Special attention was paid to the coupled-channel nature of the problem. We found a decay width of 52 keV when the tetraquark is in an isospin-0 state, using a value of $\delta m = -273$ keV, which arises from using a relativistic P-wave two-body Breit-Wigner function with a Blatt-Weisskopf form factor. This was in good agreement with the LHCb experiment. The predicted differential spectra as a function of the invariant mass of the final-state charm meson pair were also in good agreement with the binned experimental data. In this paper, we investigate how these conclusions are affected by next-to-leading-order (NLO) strong decays.

The effective theory we use is similar to the effective field theory for the $\chi_{c1}(3872)$ (XEFT) [27–41]. References [27,42,43] have considered NLO XEFT diagrams for $\chi_{c1}(3872)$ decays. One-pion exchange was found to have a negligible contribution to the decay width [27,43], while final-state rescattering leads to uncertainty in the decay rate of $^{+50\%}_{-30\%}$ when the binding energy of the $\chi_{c1}(3872)$ is 0.2 MeV [43]. The differential spectrum $d\Gamma[\chi_{c1}(3872) \to D^0\bar{D}^0\pi^0]/dE_\pi$ was found to have a curve whose peak location and overall shape are insensitive to NLO corrections; only the normalization is affected [43]. The sharply peaked nature of the differential spectrum can inform about the molecular nature of the $\chi_{c1}(3872)$: since it is a function of the virtual D^{*0} propagator $(p_D^2 + \gamma^2)^{-1}$, where γ is the binding momentum, as the binding energy goes to zero, the distribution becomes sharply peaked as $p_D \to 0$.

By analogy with this earlier work on $\chi_{c1}(3872)$, in this paper we compute NLO contributions to the decay of T_{cc}^+ to find the uncertainties due to one-loop, one-pion exchange

*lin.dai@tum.de
†spf@email.arizona.edu
‡reed.hodges@duke.edu
§mehen@duke.edu

and final-state rescattering diagrams. We calculate the uncertainty in the decay width, as well as in the shape, peak location, and normalization of differential spectra. The calculation is complicated by the presence of a coupled channel, which is not present for $\chi_{c1}(3872)$. We find the decay width including NLO corrections to be $47^{+53\%}_{-25\%}$ keV, which is consistent with XEFT [43]. We also discuss the physical significance of several of the parameters in the effective theory, and their effect on the decay width.

In Sec. II, we write down the effective Lagrangian to NLO. The required Feynman diagrams and their amplitudes, along with the explicit formulas for the partial widths are shown in Sec. III. Plots of the differential distribution are shown in Sec. IV, followed by concluding remarks in Sec. V.

II. EFFECTIVE LAGRANGIAN

The leading-order effective Lagrangian for strong decays of T_{cc}^+ is [6]

$$\begin{aligned}\mathcal{L}_{\rm LO} = {} & H^{*i\dagger}\left(i\partial^0 + \frac{\nabla^2}{2m_{H^*}} - \delta^*\right)H^{*i} + H^\dagger\left(i\partial^0 + \frac{\nabla^2}{2m_H} - \delta\right)H \\ & + \frac{g}{f_\pi}H^\dagger\partial^i\pi H^{*i} + \text{H.c.} \\ & - C_0^{(0)}(H^{*T}\tau_2 H)^\dagger(H^{*T}\tau_2 H) \\ & - C_0^{(1)}(H^{*T}\tau_2\tau_a H)^\dagger(H^{*T}\tau_2\tau_a H). \end{aligned} \tag{2}$$

Here, H and H^* are isodoublets of the pseudoscalar and vector charm meson fields, respectively, and π is the usual matrix of pion fields. The diagonal matrices δ and δ^* contain the residual masses, which are the difference between the mass of the charm meson $D^{(*)i}$, where $i = 0, +$, and that of the D^0. The coupling $g = 0.54$ is the heavy hadron chiral perturbation theory (HHχPT) axial coupling [44–46], and $f_\pi = 130$ MeV is the pion decay constant. The terms on the last two lines are contact interactions mediating D^*D scattering, where $C_0^{(n)}$ mediates S-wave scattering in the isospin-n channel, and τ_a's are Pauli matrices acting in isospin space.

Several new classes of terms appear at NLO in the effective theory. There are new contact interactions involving two derivatives:

$$\begin{aligned}\mathcal{L}_{C_2} = {} & \frac{C_2^{(0)}}{4}(H^{*T}\tau_2 H)^\dagger(H^{*T}\tau_2\overleftrightarrow{\nabla}^2 H) \\ & + \frac{C_2^{(1)}}{4}(H^{*T}\tau_2\tau_a H)^\dagger(H^{*T}\tau_2\tau_a\overleftrightarrow{\nabla}^2 H) \\ & + \text{H.c.} \end{aligned} \tag{3}$$

These interactions occur in XEFT and are proportional to the effective range [27]. We can also write down $D\pi$ interaction terms by constructing isospin invariants out of the fields:

$$\begin{aligned}\mathcal{L}_{C_\pi} = {} & C_\pi^{(1/2)}(\pi H)^\dagger(\pi H) \\ & + C_\pi^{(3/2)}\left(v_a H - \frac{1}{3}\tau_a\pi H\right)^\dagger\left(v_a H - \frac{1}{3}\tau_a\pi H\right). \end{aligned} \tag{4}$$

Here, $v = (\pi^1\ \pi^2\ \pi^0)^T/\sqrt{2}$ is a vector of pion fields, with $\pi^\pm \equiv (\pi^1 \mp i\pi^2)/\sqrt{2}$, such that $v_a\tau_a = \pi$. $C_\pi^{(1/2)}$ and $C_\pi^{(3/2)}$ mediate scattering in the isospin-1/2 and isospin-3/2 channels, respectively. The interactions which are relevant to our calculation are

$$\begin{aligned}\mathcal{L}_{C_\pi} \to {} & C_\pi^{(1)}D^{0\dagger}\pi^{0\dagger}D^+\pi^- - C_\pi^{(1)}D^{+\dagger}\pi^{0\dagger}D^0\pi^+ + \text{H.c.} \\ & + C_\pi^{(2)}D^{0\dagger}\pi^{0\dagger}D^0\pi^0 + C_\pi^{(2)}D^{+\dagger}\pi^{0\dagger}D^+\pi^0 \\ & + C_\pi^{(3)}D^{0\dagger}\pi^{+\dagger}D^0\pi^+, \end{aligned} \tag{5}$$

where the couplings $C_\pi^{(1)}$, $C_\pi^{(2)}$, and $C_\pi^{(3)}$ are particular linear combinations of $C_\pi^{(1/2)}$ and $C_\pi^{(3/2)}$ as governed by Eq. (4). These interactions can be matched onto the chiral Lagrangian [47]. The values we use for these C_π couplings are computed from lattice data; see Appendix C for details.

We can write down $D^*D \to DD\pi$ interactions by using the same strategy of constructing isospin invariants out of the fields. That would lead to

$$\begin{aligned}\mathcal{L}_{B_1} = {} & B_1^{(I=0)}\varepsilon_{\alpha\beta}(H_\alpha^* H_\beta)^\dagger(H\tau_2\tau_i H\nabla v_i) \\ & + B_1^{(I=1)}(H^*\tau_2\tau_k H)^\dagger(\varepsilon_{ijk}H\tau_2\tau_i H\nabla v_j) \\ & + \text{H.c.} \end{aligned} \tag{6}$$

However, we need isospin-breaking terms in order to fully renormalize the theory at NLO, so ultimately we have four unique B_1 couplings, one for each possible channel. Written in terms of the charm meson fields, the interactions become

$$\begin{aligned}\mathcal{L}_{B_1} \to {} & B_1^{(1)}(D^+D^{*0})^\dagger(D^+D^0\nabla\pi^0) \\ & + B_1^{(2)}(D^0D^{*+})^\dagger(D^+D^0\nabla\pi^0) \\ & + \frac{B_1^{(3)}}{2}(D^0D^{*+})^\dagger(D^0D^0\nabla\pi^+) \\ & + \frac{B_1^{(4)}}{2}(D^+D^{*0})^\dagger(D^0D^0\nabla\pi^+) \\ & + \text{H.c.} \end{aligned} \tag{7}$$

Relations between the $B_1^{(i)}$'s implied by Eq. (6) are given in Appendix C. We can construct DD contact terms out of the isospin invariants. There are only interactions in the isospin-1 channel,

$$\mathcal{L}_{C_{0D}} = C_{0D}^{(1)}(H\tau_2\tau_a H)^\dagger(H\tau_2\tau_a H) \to \frac{C_{0D}^{(1)}}{2}(D^0D^0)^\dagger(D^0D^0) + C_{0D}^{(1)}(D^+D^0)^\dagger(D^+D^0), \tag{8}$$

where in the second line we have restricted our focus to terms that are relevant to our calculation. The authors in Ref. [43] chose to vary their $C_{0D}^{(1)}$ coupling, which described $D\bar{D}$ scattering as opposed to DD, over a range of $[-1, 1]$ fm^2. We test several different values for it within that range. Lastly, we need a kinetic term for the pions; in contrast to XEFT, we treat them relativistically:

$$\mathcal{L}_\pi = \mathrm{tr}(\partial^\mu\pi^\dagger\partial_\mu\pi - m_\pi^2\pi^\dagger\pi). \tag{9}$$

The full NLO Lagrangian is then $\mathcal{L}_{\mathrm{NLO}} = \mathcal{L}_{C_2} + \mathcal{L}_{C_\pi} + \mathcal{L}_{B_1} + \mathcal{L}_{C_{0D}} + \mathcal{L}_\pi$.

III. FORMULAS FOR DECAY WIDTHS

Writing down the decay width for the T_{cc}^+ at NLO requires care due to the coupled-channel nature of the problem. We define a two-point correlation function matrix $\hat{G}$ as

$$\hat{G} = \int d^4x\, e^{-iEt}\langle 0|T[X(x)X^T(0)]|0\rangle = i\Sigma(1 + C\Sigma)^{-1}, \tag{10}$$

where the interpolating field is

$$X = \begin{pmatrix} D^0D^{*+} \\ D^+D^{*0} \end{pmatrix}. \tag{11}$$

The right-hand side of Eq. (10) arises from expressing $\hat{G}$ to all orders as an infinite sum of the C_0-irreducible two-point function Σ, in a manner similar to that in Appendix A of Ref. [48], but here C_0 and Σ are matrices due to the presence of a coupled channel. $-i\Sigma$ is given by the sum of D^*D self-energy diagrams in Fig. 1. Its diagonal elements correspond to those two-point diagrams which do not swap channels, and the off-diagonal elements to those which do swap channels. We can then project out the isospin-0 and isospin-1 channels, and tune the parameters of the two-point correlators so that there is a pole corresponding to the location of the T_{cc}^+ bound state. Near the vicinity of the pole, the Green's function can be written as

$$G_{0/1} = \begin{pmatrix} 1 \\ \mp 1 \end{pmatrix}^T \hat{G} \begin{pmatrix} 1 \\ \mp 1 \end{pmatrix} \approx \frac{1}{2}\frac{iZ_{0/1}}{E + E_T + \frac{i\Gamma_{0/1}}{2}}, \tag{12}$$

where $\Gamma_{0/1}$ is the decay width, and the residue $Z_{0/1}$ is the wave function renormalization. We find for the decay width in the isospin-0 channel

$$\Gamma_0^{\mathrm{NLO}} \approx -\Gamma^{\mathrm{LO}}\frac{\mathrm{Re}\Sigma_0'^{\mathrm{NLO}}(-E_T)}{\mathrm{Re}\,\mathrm{tr}\Sigma'^{\mathrm{LO}}(-E_T)} + \frac{2\mathrm{Im}\Sigma_0^{\mathrm{NLO}}(-E_T)}{\mathrm{Re}\,\mathrm{tr}\Sigma'^{\mathrm{LO}}(-E_T)}, \tag{13}$$

where $\Sigma_0 \equiv \Sigma_{11} + \Sigma_{22} - \Sigma_{12} - \Sigma_{21}$ is a particular combination of the elements of the Σ matrix appropriate for isospin 0. The first term of Eq. (13) is a correction to the LO decay width from NLO D^*D self-energy corrections—i.e.,

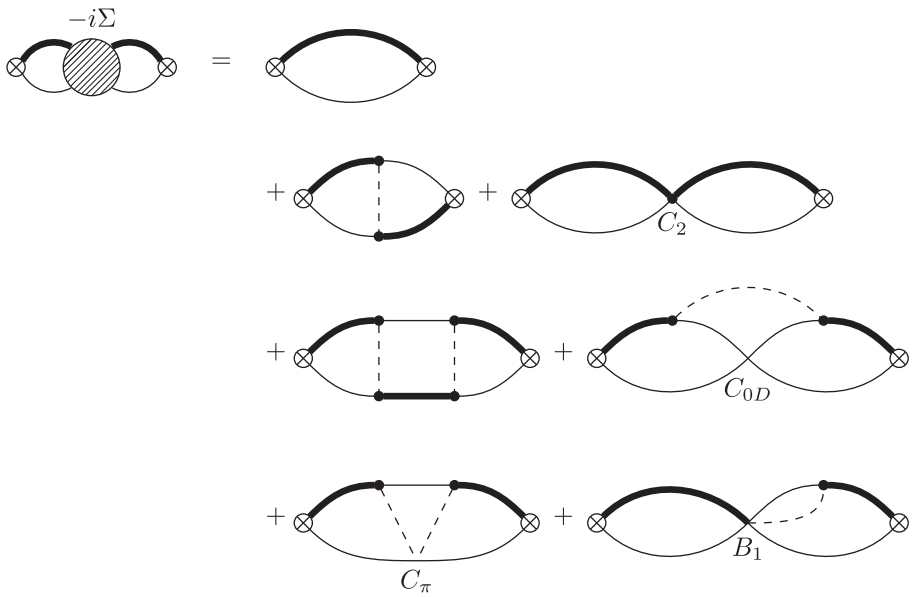

FIG. 1. Some of the D^*D self-energy diagrams contributing to $-i\Sigma$. Bold solid lines represent D^* mesons, regular solid lines represent D mesons, and dashed lines represent pions. The first row is LO, the second row is NLO, and the third and fourth rows are NNLO. There are also other NNLO diagrams not shown which are C_0-reducible combinations of the NLO diagrams.

diagrams on the second row of Fig. 1. The second term of Eq. (13) consists of NLO decay diagrams, from various cuts of diagrams on the third and fourth rows of Fig. 1. Note that $\mathrm{Im}\Sigma^{\mathrm{NLO}}$ is from Σ diagrams of 1 higher order than in $\mathrm{Re}\Sigma^{\mathrm{NLO}}$ because the LO self-energy graph has no imaginary part below threshold. The derivatives of Σ are with respect to E and evaluated at $E=-E_T$. For a more detailed derivation of Eq. (13), refer to Appendix A.

Three diagrams in Fig. 1 contribute to $\mathrm{Re}\Sigma$ to NLO. They are the LO self-energy diagram $(-i\Sigma_1)$, the one-pion exchange diagram $(-i\Sigma_2)$, and the C_2 contact diagram $(-i\Sigma_3)$. They are evaluated in the power divergence subtraction (PDS) scheme [49]. This scheme corresponds to using $\overline{\mathrm{MS}}$ to handle logarithmic divergences as well as subtracting poles in $d=3$ to keep track of linear divergences. A $1/\epsilon$ pole appears in Σ_2, but the dependence on the renormalization scale drops out when the derivative with respect to E is taken. We neglect terms in the propagators that go as $\mathbf{p}^4/m_H^2$ or $(\delta m)\mathbf{p}^2/m_H$, where δm is of the order of the pion mass, compared to $\mathbf{p}^2$. In Σ_2 and Σ_3, we use a Fourier transform to evaluate the integrals over three-momentum, using a procedure outlined in Ref. [50]. We define a reduced mass $\mu(m_1,m_2)\equiv m_1m_2/(m_1+m_2)$, and the binding momenta are defined to be $\gamma^2(m_1,m_2)=2\mu(m_1,m_2)(m_1+m_2-m_T)$. The expressions for the self-energy diagrams are

$$-i\Sigma_1(m,m^*)=-\frac{i\mu(m,m^*)}{2\pi}[\Lambda_{\mathrm{PDS}}-\gamma(m,m^*)], \tag{14}$$

$$\begin{aligned}-i\Sigma_2(m_1,m_1^*,m_2,m_2^*,m_\pi,g_1,g_2)=&-\frac{4ig_1g_2}{3}\mu(m_1,m_1^*)\mu(m_2,m_2^*)\left\{\frac{1}{16\pi^2}[\Lambda_{\mathrm{PDS}}-\gamma(m_1,m_1^*)][\Lambda_{\mathrm{PDS}}-\gamma(m_2,m_2^*)]\right.\\&+\frac{(m_2^*-m_1)^2-m_\pi^2}{(8\pi)^2}\left[\frac{1}{\epsilon}+2-4\log\left(\gamma(m_1,m_1^*)+\gamma(m_2,m_2^*)\right.\right.\\&\left.\left.\left.-i(m_2^*-m_1)^2+im_\pi^2\right)-4\log\mu\right]\right\},\end{aligned} \tag{15}$$

$$\begin{aligned}-i\Sigma_3(m_1,m_1^*,m_2,m_2^*,C_2)=&-\frac{i}{4\pi^2}C_2[\gamma^2(m_1,m_1^*)+\gamma^2(m_2,m_2^*)]\mu(m_1,m_1^*)\\&\times\mu(m_2,m_2^*)[\Lambda_{\mathrm{PDS}}-\gamma(m_1,m_1^*)][\Lambda_{\mathrm{PDS}}-\gamma(m_2,m_2^*)].\end{aligned} \tag{16}$$

To be consistent with the implementation of the PDS scheme in the decay diagrams (see Appendix B), for the double integral in Σ_2 we have used rotational symmetry to replace the tensor structure in the numerator with $\delta^{ij}/3$ and not $\delta^{ij}/(d-1)$. This choice does not affect the derivative of Σ_2, as it only changes the constant terms which drop out upon differentiation with respect to E.

The decay diagrams that contribute to $2\mathrm{Im}\Sigma_0^{\mathrm{NLO}}(-E_T)$ are shown in Fig. 2. By the optical theorem, the square of these diagrams is given by the sum over the cuts of the NNLO diagrams in Fig. 1. If there is only one pion/charm meson vertex in a diagram, its coupling is labeled g_π. If there is more than one such vertex, the couplings are numbered g_i. Depending on the type of pion and charm meson, these couplings will be either g/f_π or $\pm g/(\sqrt{2}f_\pi)$. The expressions are written in terms of the basis integrals given in Appendix B. These basis integrals depend on the parameters b, c_1, and c_2; the definitions for c_1 and c_2 are provided where appropriate, with $b=1$ unless otherwise specified; and the momentum arguments for the integrals are $\mathbf{p}$ unless otherwise specified.

$$i\mathcal{A}_{2(\mathrm{a})}(\mathbf{p},m,m^*,g_\pi)=\frac{2ig_\pi\boldsymbol{\epsilon}_T\cdot\mathbf{p}_\pi\mu(m,m^*)}{\mathbf{p}^2+\gamma^2(m,m^*)}. \tag{17}$$

$$\begin{aligned}i\mathcal{A}_{2(\mathrm{b})}(\mathbf{p},m,m_{\mathrm{ext}},m_\pi,m_1^*,m_2^*,g_1,g_2,g_3)=&\frac{4i\mu(m,m_1^*)\mu(m_{\mathrm{ext}},m_2^*)g_1g_2g_3}{\mathbf{p}^2+\gamma^2(m_{\mathrm{ext}},m_2^*)}[\boldsymbol{\epsilon}_T\cdot\mathbf{p}\mathbf{p}_\pi\cdot\mathbf{p}(I_0^{(2)}-2I^{(1)}+I)+\boldsymbol{\epsilon}_T\cdot\mathbf{p}_\pi\mathbf{p}^2I_1^{(2)}],\\c_1=&\gamma^2(m,m_1^*),\\c_2=&\mathbf{p}^2-(m_T-m-m_{\mathrm{ext}})^2+m_\pi^2.\end{aligned} \tag{18}$$

$$\begin{aligned}i\mathcal{A}_{2(\mathrm{c})}(m,m_{\mathrm{ext}},m_\pi,m^*,g_\pi,C_\pi)=&2i\mu(m,m^*)g_\pi C_\pi\boldsymbol{\epsilon}_T\cdot\mathbf{p}[I^{(1)}-I],\\c_1=&\gamma^2(m,m^*),\\c_2=&\mathbf{p}^2-(m_T-m-m_{\mathrm{ext}})^2+m_\pi^2.\end{aligned} \tag{19}$$

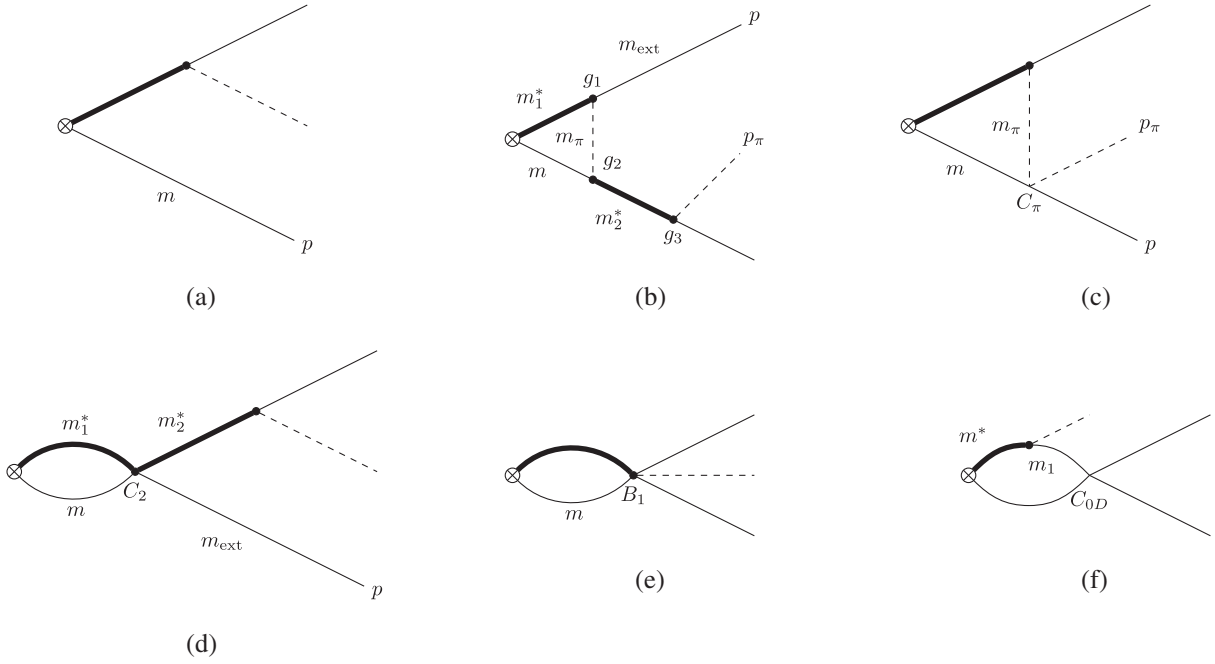

FIG. 2. Feynman diagrams at LO and NLO contributing to the decay of T_{cc}^+. We label the vertices and lines whose naming might be ambiguous. These diagrams arise from cuts of the diagrams on the third and fourth lines of Fig. 1.

$$i\mathcal{A}_{2(\mathrm{d})}(m, m_{\mathrm{ext}}, m_1^*, m_2^*, g_\pi, C_2) = \frac{1}{\pi} iC_2 g_\pi \boldsymbol{\epsilon}_T \cdot \mathbf{p}_\pi \mu(m, m_1^*)\mu(m_{\mathrm{ext}}, m_2^*) \frac{\mathbf{p}^2 - \gamma^2(m, m_1^*)}{\mathbf{p}^2 + \gamma^2(m_{\mathrm{ext}}, m_2^*)} [\gamma(m, m_1^*) - \Lambda_{\mathrm{PDS}}]. \tag{20}$$

$$i\mathcal{A}_{2(\mathrm{e})}(m, m^*, B_1) = -\frac{iB_1}{2\pi} \boldsymbol{\epsilon}_T \cdot \mathbf{p}_\pi \mu(m, m^*)[\gamma(m, m^*) - \Lambda_{\mathrm{PDS}}]. \tag{21}$$

$$\begin{aligned} i\mathcal{A}_{2(\mathrm{f})}(m_1, m_2, m^*, p_\pi^0, g_\pi, C_{0D}) &= 4i\mu(m_1, m_2)\mu(m_2, m^*) g_\pi C_{0D} \boldsymbol{\epsilon}_T \cdot \mathbf{p}_\pi I(\mathbf{p}_\pi), \\ c_1 &= \gamma^2(m_2, m^*), \\ c_2 &= -2\mu(m_1, m_2)\left(m_T - m_1 - m_2 - p_\pi^0 - \frac{\mathbf{p}_\pi^2}{2m_1}\right), \\ b &= \frac{\mu(m_1, m_2)}{m_1}. \end{aligned} \tag{22}$$

Following Eq. (13) and using the amplitudes defined above, the decay widths for the two strong decays of T_{cc}^+ are

$$\begin{aligned} \frac{d\Gamma_0^{\mathrm{NLO}}(T_{cc}^+ \to D^+ D^0 \pi^0)}{d\mathbf{p}_0^2 d\mathbf{p}_+^2} = \frac{2}{\mathrm{Re}\,\mathrm{tr}\Sigma'^{\mathrm{LO}}(-E_T)} \mathrm{Re}\Big[& \mathcal{A}_{2(\mathrm{a})}(\mathbf{p}_+, m_+, m_0^*, -g/\sqrt{2}f_\pi) \\ & \times \Big(\mathcal{A}_{2(\mathrm{b})}(\mathbf{p}_0, m_+, m_0, m_{\pi^0}, m_0^*, m_+^*, -g/\sqrt{2}f_\pi, g/\sqrt{2}f_\pi, g/\sqrt{2}f_\pi) \\ & + \mathcal{A}_{2(\mathrm{b})}(\mathbf{p}_+, m_+, m_+, m_{\pi^-}, m_0^*, m_0^*, g/f_\pi, g/f_\pi, -g/\sqrt{2}f_\pi) \\ & - \mathcal{A}_{2(\mathrm{b})}(\mathbf{p}_0, m_0, m_0, m_{\pi^+}, m_+^*, m_+^*, g/f_\pi, g/f_\pi, g/\sqrt{2}f_\pi) \\ & - \mathcal{A}_{2(\mathrm{b})}(\mathbf{p}_+, m_0, m_+, m_{\pi^0}, m_+^*, m_0^*, g/\sqrt{2}f_\pi, -g/\sqrt{2}f_\pi, -g/\sqrt{2}f_\pi) \\ & + \mathcal{A}_{2(\mathrm{c})}(\mathbf{p}_0, m_+, m_0, m_{\pi^0}, m_0^*, -g/\sqrt{2}f_\pi, C_\pi^{(2)}) \\ & - \mathcal{A}_{2(\mathrm{c})}(\mathbf{p}_0, m_0, m_0, m_{\pi^+}, m_+^*, g/f_\pi, C_\pi^{(1)}) + \mathcal{A}_{2(\mathrm{f})}(m_0, m_+, m_0^*, -g/\sqrt{2}f_\pi, C_{0D}^{(1)}) \\ & - \mathcal{A}_{2(\mathrm{f})}(m_+, m_0, m_+^*, g/\sqrt{2}f_\pi, C_{0D}^{(1)}) \Big)^* + (D^0 \leftrightarrow D^+, \pi^+ \leftrightarrow \pi^-) \Big] \end{aligned}$$

$$
\begin{aligned}
&- \frac{1}{\mathrm{Re\,tr}\Sigma'^{\mathrm{LO}}(-E_T)}\Big[[\beta_1(\mathbf{p}_+^2+\gamma_+^2)+\beta_2](|\mathcal{A}_{2(\mathrm{a})}(\mathbf{p}_+,m_+,m_0^*,-g/\sqrt{2}f_\pi)|^2 \\
&- \mathcal{A}_{2(\mathrm{a})}(\mathbf{p}_0,m_0,m_+^*,g/\sqrt{2}f_\pi)\mathcal{A}^*_{2(\mathrm{a})}(\mathbf{p}_+,m_+,m_0^*,-g/\sqrt{2}f_\pi)) \\
&+ [\beta_3(\mathbf{p}_0^2+\gamma_0^2)+\beta_4](|\mathcal{A}_{2(\mathrm{a})}(\mathbf{p}_0,m_0,m_+^*,g/\sqrt{2}f_\pi)|^2 \\
&- \mathcal{A}_{2(\mathrm{a})}(\mathbf{p}_+,m_+,m_0^*,-g/\sqrt{2}f_\pi)\mathcal{A}^*_{2(\mathrm{a})}(\mathbf{p}_0,m_0,m_+^*,g/\sqrt{2}f_\pi))\Big] \\
&- \frac{d\Gamma_0^{\mathrm{LO}}(T_{cc}^+\to D^+D^0\pi^0)}{d\mathbf{p}_0^2 d\mathbf{p}_+^2}\frac{\mathrm{Re}\Sigma_0'^{\mathrm{NLO}}}{\mathrm{Re\,tr}\Sigma'^{\mathrm{LO}}}\bigg|_{C_2\to 0,E=-E_T},
\end{aligned}
\tag{23}
$$

$$
\begin{aligned}
\frac{d\Gamma_0^{\mathrm{NLO}}(T_{cc}^+\to D^0D^0\pi^+)}{d\mathbf{p}_1^2 d\mathbf{p}_2^2} &= \frac{1}{\mathrm{Re\,tr}\Sigma'^{\mathrm{LO}}(-E_T)}\mathrm{Re}\Big[\mathcal{A}_{2(\mathrm{a})}(\mathbf{p}_2,m_0,m_+^*,g/f_\pi) \\
&\times\Big(\mathcal{A}_{2(\mathrm{b})}(\mathbf{p}_1,m_0,m_0,m_{\pi^+},m_+^*,m_+^*,g/f_\pi,g/f_\pi,g/f_\pi) \\
&+ \mathcal{A}_{2(\mathrm{b})}(\mathbf{p}_2,m_0,m_0,m_{\pi^+},m_+^*,m_+^*,g/f_\pi,g/f_\pi,g/f_\pi) \\
&- \mathcal{A}_{2(\mathrm{b})}(\mathbf{p}_1,m_+,m_0,m_{\pi^0},m_0^*,m_+^*,-g/\sqrt{2}f_\pi,g/\sqrt{2}f_\pi,g/f_\pi) \\
&- \mathcal{A}_{2(\mathrm{b})}(\mathbf{p}_2,m_+,m_0,m_{\pi^0},m_0^*,m_+^*,-g/\sqrt{2}f_\pi,g/\sqrt{2}f_\pi,g/f_\pi) \\
&+ \mathcal{A}_{2(\mathrm{c})}(\mathbf{p}_1,m_0,m_0,m_{\pi^+},m_+^*,g/f_\pi,C_\pi^{(3)}) - \mathcal{A}_{2(\mathrm{c})}(\mathbf{p}_1,m_+,m_0,m_{\pi^0},m_0^*,-g/\sqrt{2}f_\pi,C_\pi^{(1)}) \\
&+ \mathcal{A}_{2(\mathrm{f})}(m_0,m_0,m_+^*,g/f_\pi,C_{0D}^{(1)}/2)\Big)^* + (\mathbf{p}_1\leftrightarrow\mathbf{p}_2) - \left(\frac{2g\mu_0}{f_\pi}\right)^2\frac{\mathbf{p}_\pi^2}{3}\beta_5\left(\frac{1}{\mathbf{p}_1^2+\gamma_0^2}+\frac{1}{\mathbf{p}_2^2+\gamma_0^2}\right)\Big] \\
&- \frac{d\Gamma_0^{\mathrm{LO}}(T_{cc}^+\to D^0D^0\pi^+)}{d\mathbf{p}_1^2 d\mathbf{p}_2^2}\left(\beta_4+\frac{\mathrm{Re}\Sigma_0'^{\mathrm{NLO}}}{\mathrm{Re\,tr}\Sigma'^{\mathrm{LO}}}\bigg|_{C_2\to 0,E=-E_T}\right).
\end{aligned}
\tag{24}
$$

In the previous formulas, we have used subscripts on μ and γ to indicate which charm meson is a pseudoscalar in that particular channel—e.g., $\mu_0=\mu(m_0,m_+^*)$. The combinations of self-energy diagrams that we need are $\mathrm{Re\,tr}\Sigma'^{\mathrm{LO}}(-E_T)$ and $\mathrm{Re}\Sigma_0'^{\mathrm{NLO}}(-E_T,C_2\to 0)$. In terms of the functions defined above, these are given by

$$
\begin{aligned}
\mathrm{Re\,tr}\Sigma'^{\mathrm{LO}} &= \mathrm{Re}\Sigma_1'(m_0,m_+^*)+\mathrm{Re}\Sigma_1'(m_+,m_0^*), \\
\mathrm{Re}\Sigma_0'^{\mathrm{NLO}}|_{C_2\to 0} &= \mathrm{Re}\Big[\Sigma_2'(m_+,m_0^*,m_+,m_0^*,m_{\pi^+},g/f_\pi,g/f_\pi)+\Sigma_2'(m_0,m_+^*,m_0,m_+^*,m_{\pi^+},g/f_\pi,g/f_\pi) \\
&\quad+\Sigma_2'(m_+,m_0^*,m_0,m_+^*,m_{\pi^0},-g/\sqrt{2}f_\pi,g/\sqrt{2}f_\pi)+\Sigma_2'(m_0,m_+^*,m_+,m_0^*,m_{\pi^0},g/\sqrt{2}f_\pi,-g/\sqrt{2}f_\pi)\Big].
\end{aligned}
\tag{25}
$$

The expressions for β_i are given in Appendix C. The terms dependent on $\mathcal{A}_{(2\mathrm{b})}$ and $\mathrm{Re}\Sigma_2'$ have linear divergences that must cancel against each other. They cancel exactly in the limit $\mu_0=\mu_+$. We make that approximation in those terms only to ensure the cancellation; it is a reasonable approximation as $\mu_0/\mu_+\approx 0.99948$. See Appendix B for more discussion of these linear divergences.

IV. DIFFERENTIAL DECAY DISTRIBUTIONS AND PARTIAL WIDTHS

Once we have formulas for the $T_{cc}^+\to DD\pi$ partial widths, we can numerically integrate over part of the three-body phase space in *Mathematica* and plot the differential distribution $d\Gamma/dm_{DD}$. It is insightful to compare our predicted curves to the LHCb experimental data for the total yield. This will inform us about the effect and importance of the different interactions in the effective theory. We normalize our distributions by performing a least-squares fit of the LO distribution to the data, and using the same normalization factor for the NLO distributions. The C_π decay diagrams, individually and as a whole, contribute negligibly to the distributions. The parameters β_1, β_3, and β_5 also have a small impact on the distributions over the range in which we vary them. We therefore do not show plots varying these parameters individually.

The contributions from the non-C_2-dependent NLO self-energy corrections (i.e., the first diagram on the second line of Fig. 1), as well as the contributions from Fig. 2(b), serve to increase the partial widths by a small but noticeable amount (Fig. 3). The effect of the C_{0D}, β_2, and β_4 terms on the distributions can be significant. In the following, we will investigate their impact by setting all other contributions to $d\Gamma_{\mathrm{NLO}}/dm_{DD}$ to zero and varying them individually.

The C_{0D} interaction has a sizeable contribution to the partial widths, as evidenced in Fig. 4, where we plot the differential distributions and vary this coupling in two

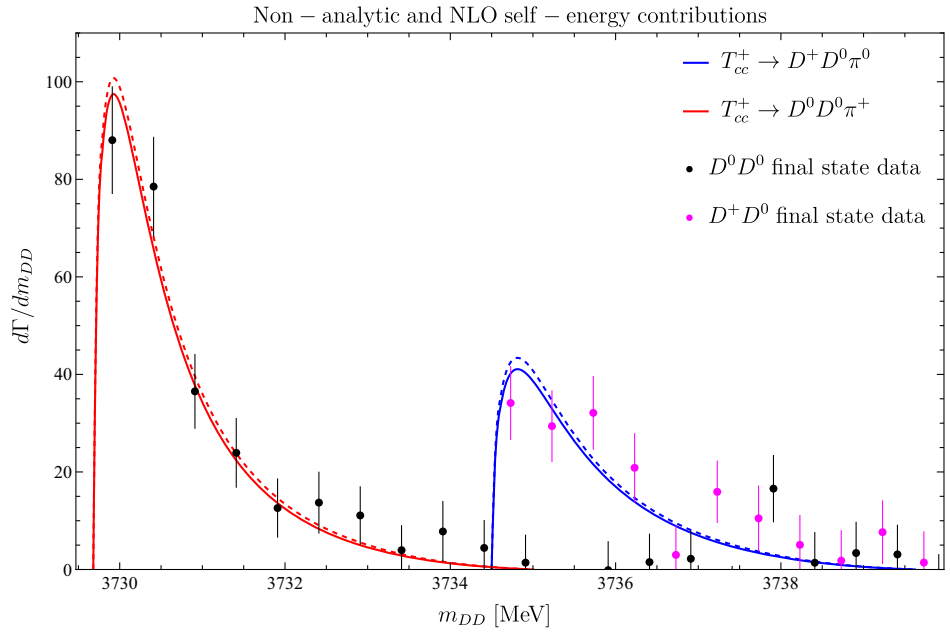

FIG. 3. A plot of the differential decay width as a function of the invariant mass of the final-state D-meson pair. Solid lines represent the LO calculation; the dashed lines represent the addition of nonanalytic and NLO self-energy corrections. Overlaid are the binned experimental data from LHCb, with the background subtracted.

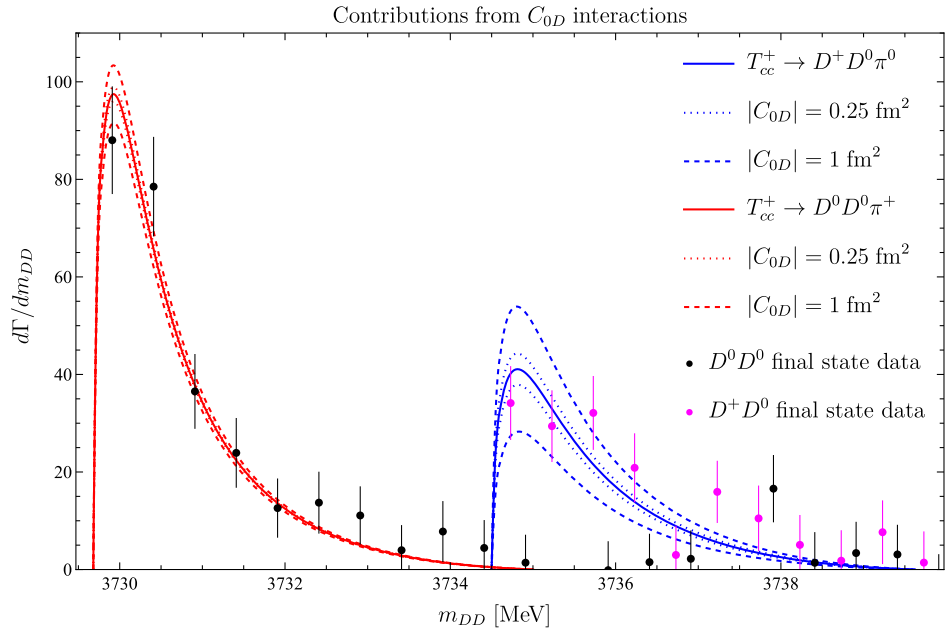

FIG. 4. A plot of the differential decay width as a function of the invariant mass of the final-state D-meson pair. Solid lines represent the LO calculation; the dashed and dotted lines represent two different ranges for C_{0D}. Overlaid are the binned experimental data from LHCb, with the background subtracted.

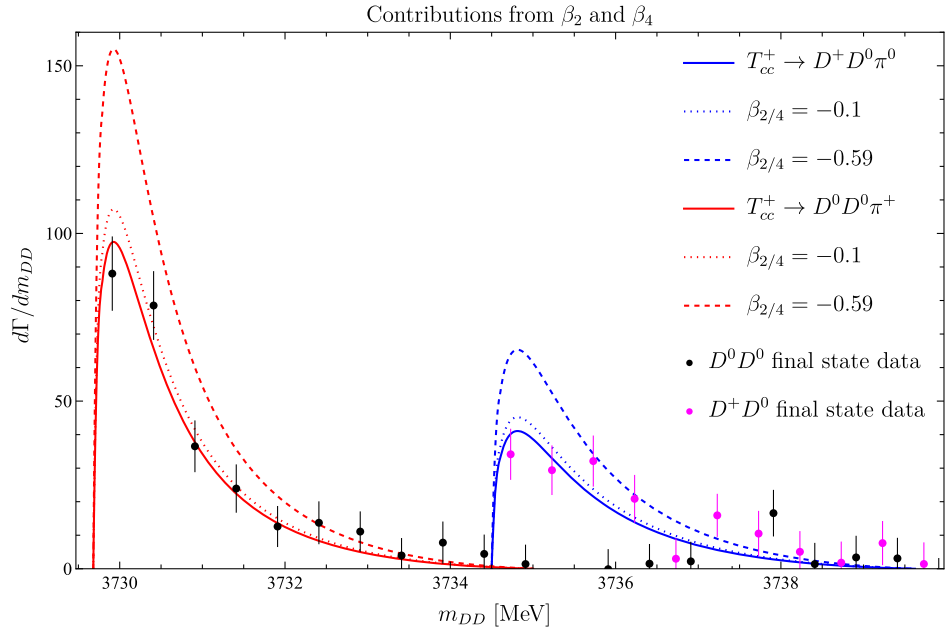

FIG. 5. A plot of the differential decay width as a function of the invariant mass of the final-state D-meson pair. Solid lines represent the LO calculation. The dashed and dotted lines represent two different values of β_2 and β_4. Overlaid are the binned experimental data from LHCb, with the background subtracted.

possible ranges: $C_{0D} \in [-1, 1]\,\mathrm{fm}^2$ and $\in [-0.25, 0.25]\,\mathrm{fm}^2$. Its effect on the neutral pion decay is twice as large as on the charged pion decay, because the coupling of charged pions to D mesons is bigger by a factor of $\sqrt{2}$. Clearly, the differential distributions are sensitive to the coupling's magnitude. If C_{0D} is $+1$ fm^2, the peak of the D^+D^0 mass distribution is too high, and if it is -1 fm^2, then three higher data points are underpredicted. It would be interesting to perform a more careful analysis of the constraints these data put on C_{0D}, but that is beyond the scope of this paper. C_{0D} is directly proportional to the $I = 1$ D-meson scattering length, so more precise knowledge of C_{0D} from lattice simulations or experiments would allow us to sharpen our predictions for T_{cc}^+.

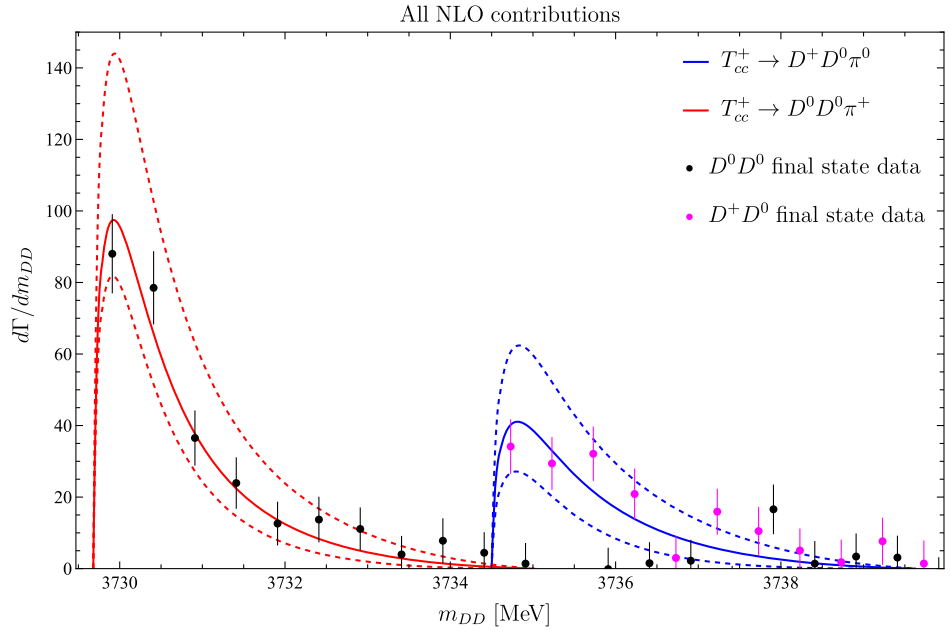

FIG. 6. A plot of the differential decay width as a function of the invariant mass of the final-state D-meson pair. Solid lines represent LO calculation; the dashed lines represent the lower and upper bounds of the NLO corrections. Here, we vary $-1\ \mathrm{fm}^2 \le C_{0D} \le 0.25\ \mathrm{fm}^2$ and $-0.26 \le \beta_{2/4} \le 0$. Overlaid are the binned experimental data from LHCb, with the background subtracted.

TABLE I. Partial and total widths in units of keV at LO and NLO.

	LO result	NLO lower bound	NLO upper bound
$\Gamma[T_{cc}^+ \to D^0 D^0 \pi^+]$	28	21	44
$\Gamma[T_{cc}^+ \to D^+ D^0 \pi^0]$	13	7.8	21
$\Gamma_{\text{strong}}[T_{cc}^+]$	41	29	66
$\Gamma_{\text{strong}}[T_{cc}^+] + \Gamma_{\text{EM}}^{\text{LO}}[T_{cc}^+]$	47	35	72

We can glean the significance of β_2 and β_4 by taking the isospin limit $m_0 = m_+$. In Appendix C, we see that in this limit,

$$\beta_2 = \beta_4 = -\gamma r_0, \tag{26}$$

where γ is the binding momentum and r_0 is the effective range in the $I = 0$ channel. The effective range is positive, and we expect $\gamma r_0 < 1$. In Fig. 5, we plot the distribution with all other NLO interactions turned off, and for two values of $\beta_2 = \beta_4 \equiv \beta$: -0.1 and -0.59, along with the LO curve ($\beta = 0$). We get $\gamma r_0 = 0.59$ if we use the largest binding momentum (γ_+) and $r_0 = 1/(100\ \text{MeV})$. For nucleons, $r_0 \approx 1/(100\ \text{MeV})$; since charm mesons are considerably more compact objects, one might expect the effective range for charm mesons to be smaller. We can see that the distribution is highly sensitive to the choice of β. A β of -0.59 greatly increases the differential distribution and is in much poorer agreement with the experimental data. This suggests that the effective range for T_{cc}^+ is smaller than for nucleons.

Clearly, the partial widths and their differential distributions can vary substantially depending on the choice of parameters in the effective field theory. However, the availability of experimental data for the decays presents the possibility of performing fits of the distributions to the data to obtain estimates for these parameters. This could improve the predictive power of the effective theory. We save such a careful statistical analysis for a future publication.

We can use these plots that show the effect of a subset of the NLO contributions to inform which ranges for the parameters to use when estimating the total NLO contribution to the differential distribution (Fig. 6). The upper and lower bounds in the figure reflect varying C_{0D} from $-1\ \text{fm}^2$ to $0.25\ \text{fm}^2$. The parameters β_1, β_3, and β_5 are varied from $-1/(100\ \text{MeV})^2$ to $+1/(100\ \text{MeV})^2$. The parameters β_2 and β_4, which reduce to $-\gamma r_0$ in the isospin limit, are varied between 0 and -0.26. The latter value corresponds to a binding momentum for the $D^{*+}D^0$ channel, γ_0, and $r_0 = 1/(100\ \text{MeV})$. While the uncertainty in the total width of the T_{cc}^+ can be significant depending on the values of the NLO couplings, the qualitative aspects of the plots of the differential decay widths in Fig. 6 are consistent between LO and NLO. The overall shape and location of the peaks are unchanged by pion exchange and final-state rescattering.

When integrating over the full phase space to get the partial widths, we use the same ranges for the parameters as in Fig. 6. The partial widths are given in Table I. Note that the LO numbers differ from those in our original paper [6] because here we use the binding energy from the unitarized Breit-Wigner fit, whereas in Ref. [6] we used the value from the P-wave two-body Breit-Wigner fit with a Blatt-Weisskopf form factor. This has the effect of slightly increasing the prediction for the width compared to the initial paper, bringing it closer to the experimental value. When adding the LO electromagnetic decay width of

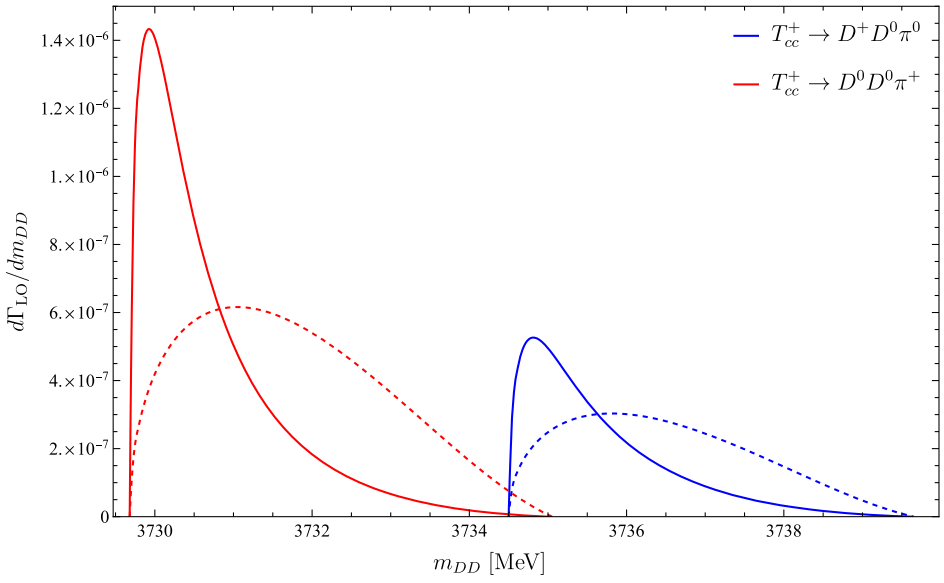

FIG. 7. Comparing our LO differential decay width to one where the D^* propagators are taken to be constant. The curves are fixed to have the same normalization. Note the lack of a sharp peak in the constant propagator curves.

6.1 keV (which is only slightly affected by the different binding energy), the total LO width predicted by our effective theory is 47 keV, which is already in excellent agreement with the LHCb experimental value of 48 keV. Adding in the NLO contribution to the strong decay widths, the total width of the T_{cc}^+ can range from 35 keV to 72 keV. Therefore, we can establish an uncertainty in the width due to NLO strong decays of $\Gamma[T_{cc}^+] = 47^{+53\%}_{-25\%}$ keV. This is comparable to the uncertainty from similar operators contributing to the decay of $\chi_{c1}(3872)$ in XEFT [43].

We did not consider NLO corrections to the electromagnetic decay, because the LO electromagnetic decay was already a small contribution to the total width. In particular, the differential distribution for the electromagnetic decay was negligible compared to the strong decays' distributions.

To illustrate why these differential decay width plots are good tests of the molecular nature of the T_{cc}^+, in Fig. 7 we can compare the LO differential curves to those which would arise if we replaced the virtual D^* propagators with a constant. The latter do not have sharp peaks and thus would be in poor agreement with the experimental data.

V. CONCLUSIONS

In this paper, we have determined the effects of NLO strong decays on the total width and differential decay width of the exotic meson T_{cc}^+. We considered pion exchange and final-state rescattering diagrams from similar operators to those in XEFT for the $\chi_{c1}(3872)$ [43]. We arrived at similar conclusions to Ref. [43]. The differential decay width plots have shapes and peaks that are relatively unchanged by the NLO effects, but the total width has significant uncertainty: $\Gamma[T_{cc}^+] = 47^{+53\%}_{-25\%}$ keV. The central value (the LO result) is in good agreement with data.

We varied the parameters in the NLO calculation to get a sense of the uncertainty in the predictions and determine which parameters in the NLO calculation give the biggest corrections. Nonanalytic corrections for pion loops are not important. The parameter C_{0D}, which is proportional to the $I = 1$ D-meson scattering length, and β_2 and β_4, which in the isospin limit are equal and proportional to the $I = 0$ D-meson effective ranges, significantly affect the decay width and normalization of the differential distribution. It would be interesting to fit the NLO differential curves to the experimental data and obtain bounds on the undetermined couplings, thereby learning more about these physical quantities. Alternatively, one might hope to get information about these parameters from lattice simulations or other experiments. Any improvement in our understanding of these parameters in D-meson scattering would increase the predictive power of the effective field theory.

ACKNOWLEDGMENTS

L. D. is supported by the Alexander von Humboldt Foundation. S. F. is supported by the U.S. Department of Energy, Office of Science, Office of Nuclear Physics, under Award No. DE-FG02-04ER41338. T. M. and R. H. are supported by the U.S. Department of Energy, Office of Science, Office of Nuclear Physics under Grant Contract No. DE-FG02-05ER41367.

APPENDIX A: COUPLED-CHANNEL DECAY WIDTH

The full expression for the isospin-0 two-point correlator is

$$-iG_0 = \frac{-\frac{1}{2}\Sigma_0 - 2C_0^{(1)}\det\Sigma}{1 + C_0^{(0)}\Sigma_0 + C_0^{(1)}\Sigma_1 + 4C_0^{(0)}C_0^{(1)}\det\Sigma}, \quad \text{(A1)}$$

where $\Sigma_{0/1} \equiv \Sigma_{11} + \Sigma_{22} \mp \Sigma_{12} \mp \Sigma_{21}$ are the isospin-0 and isopsin-1 combinations of the elements of Σ. Since we expect T_{cc}^+ to be an isospin-0 state, we treat $C_0^{(1)}$ perturbatively and expand to NLO in $C_0^{(1)}$:

$$-iG_0 \approx \frac{1}{2}\frac{-\Sigma_0}{1 + C_0^{(0)}\Sigma_0} + \frac{1}{2}\frac{C_0^{(1)}(\Sigma_{11}^{\rm LO} - \Sigma_{22}^{\rm LO})^2}{(1 + C_0^{(0)}\Sigma_0)^2}. \quad \text{(A2)}$$

We see that the real numerator of the $C_0^{(1)}$ term is the residue of a double pole at $1 + C_0^{(0)}\Sigma_0 = 0$. That can be interpreted physically as a small shift in the location of the bound state, which can be seen from expanding the right-hand side of Eq. (12) about $E_T^{\rm NLO} = E_T - E_T^{\rm LO}$. But since we are already tuning E_T to be the location of the T_{cc}^+ bound state, we can set $C_0^{(1)}$ to zero to remove the double pole from the amplitude:

$$-iG_0 \to \frac{1}{2}\frac{-\Sigma_0}{1 + C_0^{(0)}\Sigma_0}. \quad \text{(A3)}$$

At this stage, the problem is identical to the single-channel problem in XEFT [27], with the single-channel two-point function replaced by our isospin-0 combination of coupled-channel two-point functions. The wave function renormalization and decay width are therefore

$$Z_0 = \frac{1}{(C_0^{(0)})^2 {\rm Re}\Sigma_0'(-E_T)},$$
$$\Gamma_0 = \frac{2{\rm Im}\Sigma_0(-E_T)}{{\rm Re}\Sigma_0'(-E_T)}. \quad \text{(A4)}$$

Σ_0 has LO contributions from the diagonal elements, and NLO contributions from all elements. After expanding in the NLO terms, we find our corrections to the LO decay width:

$$\Gamma_0 \approx \Gamma^{\rm LO}\left(1 - \frac{{\rm Re}\Sigma_0'^{\rm NLO}(-E_T)}{{\rm Re}{\rm tr}\Sigma'^{\rm LO}(-E_T)}\right) + \frac{2{\rm Im}\Sigma_0^{\rm NLO}(-E_T)}{{\rm Re}{\rm tr}\Sigma'^{\rm LO}(-E_T)}. \quad \text{(A5)}$$

APPENDIX B: BASIS INTEGRALS AND THE PDS SCHEME

The most basic integral that arises when evaluating the one-loop diagrams in the PDS scheme is

$$\left(\frac{\Lambda_{\rm PDS}}{2}\right)^{4-d}\int\frac{d^{d-1}\mathbf{l}}{(2\pi)^{d-1}}\frac{1}{\mathbf{l}^2+c-i\epsilon}=\frac{1}{4\pi}(\Lambda_{\rm PDS}-\sqrt{c-i\epsilon}). \tag{B1}$$

This result is obtained by subtracting the pole in $d=3$ with a counterterm, then evaluating the result in $d=4$, yielding a linear divergence in $\Lambda_{\rm PDS}$.

The scalar integral $I(\mathbf{p})$ is finite in $d=3$ and $d=4$, so no PDS counterterm is needed:

$$\begin{aligned}I(\mathbf{p})&=\int\frac{d^{d-1}\mathbf{l}}{(2\pi)^{d-1}}\frac{1}{\mathbf{l}^2+c_1-i\epsilon}\frac{1}{\mathbf{l}^2-2b\mathbf{l}\cdot\mathbf{p}+c_2-i\epsilon}\\&=\frac{1}{8\pi}\frac{1}{\sqrt{b^2\mathbf{p}^2}}\left[\tan^{-1}\left(\frac{c_2-c_1}{2\sqrt{b^2\mathbf{p}^2c_1}}\right)\right.\\&\quad\left.+\tan^{-1}\left(\frac{2b^2\mathbf{p}^2+c_1-c_2}{2\sqrt{b^2\mathbf{p}^2(c_2-b^2\mathbf{p}^2)}}\right)\right].\end{aligned} \tag{B2}$$

The linear tensor integral $I^{(1)}(\mathbf{p})$ can be solved using algebraic manipulation of the numerator, which yields two integrals of the form of Eq. (B1) that have opposite signs for the divergence, and so $I^{(1)}(\mathbf{p})$ is UV-finite:

$$\begin{aligned}\mathbf{p}^iI^{(1)}(\mathbf{p})&=\int\frac{d^{d-1}\mathbf{l}}{(2\pi)^{d-1}}\mathbf{l}^i\frac{1}{\mathbf{l}^2+c_1-i\epsilon}\frac{1}{\mathbf{l}^2-2b\mathbf{l}\cdot\mathbf{p}+c_2-i\epsilon},\\\rightarrow\mathbf{p}^2I^{(1)}(\mathbf{p})&=\frac{1}{2b}\left[\frac{1}{4\pi}\sqrt{c_1-i\epsilon}-\frac{1}{4\pi}\sqrt{c_2-b^2\mathbf{p}^2-i\epsilon}\right.\\&\quad\left.+(c_2-c_1)I(\mathbf{p})\right].\end{aligned} \tag{B3}$$

The quadratic tensor integrals $I^{(2)}$ require care when implementing the PDS scheme. The linear divergences which arise in the decay width can only cancel if the subtraction scheme is implemented correctly. After using Feynman parameters to combine the propagators and obtain an integrand like $\mathbf{l}^i\mathbf{l}^jf(\mathbf{l}^2)$, the correct procedure is to replace $\mathbf{l}^i\mathbf{l}^j\to\delta^{ij}/3$ immediately, and not with $\delta^{ij}/(d-1)$. The latter would cancel the factor of $d-1$ that arises when evaluating the loop momentum integral, and this results in the incorrect coefficient for the PDS subtraction scale $\Lambda_{\rm PDS}$. Additionally, algebraic manipulation of the numerator of $I^{(2)}$ to reduce it to integrals of the form of $I^{(1)}$ and I leads to yet another incorrect coefficient. This is the method used to obtain the expressions in the Appendix of Ref. [43]; as such, the formulas for the decay width in that paper are only correct if $\Lambda_{\rm PDS}=0$ and $d=4$.

Using the correct procedure for the basis integrals gives the following results:

$$\begin{aligned}&\mathbf{p}^i\mathbf{p}^jI_0^{(2)}(\mathbf{p})+\delta^{ij}\mathbf{p}^2I_1^{(2)}(\mathbf{p})\\&\quad=\int\frac{d^{d-1}\mathbf{l}}{(2\pi)^{d-1}}\mathbf{l}^i\mathbf{l}^j\frac{1}{\mathbf{l}^2+c_1-i\epsilon}\frac{1}{\mathbf{l}^2-2b\mathbf{l}\cdot\mathbf{p}+c_2-i\epsilon},\\&I_0^{(2)}(\mathbf{p})=\frac{b^2}{8\pi}\int_0^1dx\frac{x^2}{\sqrt{\Delta(x)}},\\&\rightarrow\mathbf{p}^2I_1^{(2)}(\mathbf{p})=\frac{1}{8\pi}\left[\frac{2}{3}\Lambda_{\rm PDS}-\int_0^1dx\sqrt{\Delta(x)}\right],\end{aligned} \tag{B4}$$

for $\Delta(x)=-b^2\mathbf{p}^2x^2+(c_2-c_1)x+c_1-i\epsilon$. One can be reassured that this implementation of the PDS scheme is correct because the same relative weight of the $\Lambda_{\rm PDS}$ and $\int_0^1dx\sqrt{\Delta(x)}$ terms is obtained when using a hard cutoff. That does not occur when using $\mathbf{l}^i\mathbf{l}^j\to\delta^{ij}/(d-1)$ or algebraic manipulation of the numerator. Furthermore, unless the relative weight of the cutoff-dependent terms in $I_1^{(2)}$ and $\mathrm{Re}\Sigma_2'$ is $2/3$, the linear divergences that appear in $\Gamma_0^{\rm NLO}$ as $\mathcal{A}_{(2b)}$ and $\mathrm{Re}\Sigma_2'$ do not cancel in the isospin limit, as they do in XEFT. For the T_{cc}^+, they cancel when $\mu_0=\mu_+$, an approximation we make in the cutoff-dependent terms to ensure cancellation.

With algebraic manipulation of the integrand in $I_0^{(2)}$ and integration by parts in $I_1^{(2)}$, we can rewrite these expressions in terms of I and $I^{(1)}$:

$$\begin{aligned}\mathbf{p}^2I_0^{(2)}&=-\frac{1}{16\pi}\sqrt{c_2-b^2\mathbf{p}^2-i\epsilon}+\frac{c_1}{2}I(\mathbf{p})\\&\quad+\frac{3}{4}\frac{c_2-c_1}{b}I^{(1)}(\mathbf{p}),\\\mathbf{p}^2I_1^{(2)}&=\frac{\Lambda_{\rm PDS}}{12\pi}-\frac{1}{16\pi}\sqrt{c_2-b^2\mathbf{p}^2-i\epsilon}\\&\quad-\frac{c_1}{2}I(\mathbf{p})-\frac{1}{4}\frac{c_2-c_1}{b}I^{(1)}(\mathbf{p}).\end{aligned} \tag{B5}$$

APPENDIX C: C_π COUPLINGS AND β_i EXPRESSIONS

In the isospin $|I,m_I\rangle$ basis, we use the phase convention

$$\begin{aligned}|\pi^+\rangle&=-|1,1\rangle,&|\pi^0\rangle&=|1,0\rangle,\\|D^+\rangle&=\left|\frac{1}{2},\frac{1}{2}\right\rangle,&|D^0\rangle&=\left|\frac{1}{2},-\frac{1}{2}\right\rangle.\end{aligned} \tag{C1}$$

Then, the Clebsch-Gordan decomposition of the $D\pi$ pairs is

$$|D^0\pi^0\rangle = \sqrt{\frac{2}{3}}\left|\frac{3}{2},-\frac{1}{2}\right\rangle + \frac{1}{\sqrt{3}}\left|\frac{1}{2},-\frac{1}{2}\right\rangle,$$
$$|D^+\pi^0\rangle = \sqrt{\frac{2}{3}}\left|\frac{3}{2},\frac{1}{2}\right\rangle + \frac{1}{\sqrt{3}}\left|\frac{1}{2},\frac{1}{2}\right\rangle,$$
$$|D^0\pi^+\rangle = -\sqrt{\frac{2}{3}}\left|\frac{1}{2},\frac{1}{2}\right\rangle - \frac{1}{\sqrt{3}}\left|\frac{3}{2},\frac{1}{2}\right\rangle. \tag{C2}$$

From this, we can deduce

$$a_{D^0\pi^0} = a_{D^+\pi^0} = \frac{2}{3}a_{D_\pi}^{3/2} + \frac{1}{3}a_{D\pi}^{1/2},$$
$$a_{D^0\pi^+} = \frac{1}{3}a_{D\pi}^{3/2} + \frac{2}{3}a_{D\pi}^{1/2}. \tag{C3}$$

These scattering lengths are calculated on the lattice in Ref. [51] to be $a_{D\pi}^{1/2} = 0.37^{+0.03}_{-0.02}$ fm and $a_{D\pi}^{3/2} = -(0.100 \pm 0.002)$ fm. The matching from tree-level scattering tells us that, for the diagonal couplings $C_\pi^{(2)}$ and $C_\pi^{(3)}$, we can use $C_\pi = 4\pi(1 + m_\pi/m_D)a_{D\pi}$, with the appropriate masses and scattering lengths for each process. We can then use those two values to solve for $C_\pi^{(1/2)}$ and $C_\pi^{(3/2)}$ and obtain $C_\pi^{(1)}$. We get

$$C_\pi^{(1)} = -3.0^{+0.32}_{-0.40}\ \text{fm},$$
$$C_\pi^{(2)} = -0.76^{+0.14}_{-0.09}\ \text{fm},$$
$$C_\pi^{(3)} = 2.9^{+0.3}_{-0.2}\ \text{fm}. \tag{C4}$$

The expressions for the β_i's are given below. The subscripts on the γ and μ variables indicate the pseudoscalar charm meson is in that channel—e.g., $\gamma_+ = \gamma(m_+, m_0^*)$ is the binding momentum in the channel with the D^+ meson.

$$\beta_1 = (\Lambda_{\rm PDS} - \gamma_+)\left(\frac{f_\pi}{\sqrt{2}\pi g}B_1^{(1)} + \frac{1}{\pi}C_2^{(+)}\mu_+ - \frac{1}{\pi}C_2^{(-)}\mu_0\frac{\Lambda_{\rm PDS} - \gamma_0}{\Lambda_{\rm PDS} - \gamma_+}\right), \tag{C5}$$

$$\begin{aligned}\beta_2 = \Bigg[&\frac{1}{\pi}C_2^{(+)}\mu_+(-2\gamma_+^2)(\Lambda_{\rm PDS} - \gamma_+) - \frac{1}{\pi}C_2^{(-)}\mu_0(-\gamma_0^2 - \gamma_+^2)(\Lambda_{\rm PDS} - \gamma_0)\\ &+ 2\pi\left(\frac{\mu_0^2}{\gamma_0} + \frac{\mu_+^2}{\gamma_+}\right)^{-1}\Bigg[-\frac{1}{\pi^2}C_2^{(+)}\mu_+^3(\gamma_+ - \Lambda_{\rm PDS})(2\gamma_+ - \Lambda_{\rm PDS}) - \frac{1}{\pi^2}C_2^{(+)}\mu_0^3(\gamma_0 - \Lambda_{\rm PDS})(2\gamma_0 - \Lambda_{\rm PDS})\\ &- \frac{C_2^{(-)}(\gamma_+^2 + \gamma_0^2)\mu_+\mu_0}{2\pi}\left(\frac{\mu_+}{\gamma_0}(\Lambda_{\rm PDS} - \gamma_0) + \frac{\mu_0}{\gamma_+}(\Lambda_{\rm PDS} - \gamma_+)\right) + \frac{C_2^{(-)}\mu_+\mu_0(\mu_+ + \mu_0)}{\pi^2}(\Lambda_{\rm PDS} - \gamma_+)(\Lambda_{\rm PDS} - \gamma_0)\Bigg]\Bigg],\end{aligned} \tag{C6}$$

$$\beta_3 = (\Lambda_{\rm PDS} - \gamma_0)\left(-\frac{f_\pi}{\sqrt{2}\pi g}B_1^{(2)} + \frac{1}{\pi}C_2^{(+)}\mu_0 - \frac{1}{\pi}C_2^{(-)}\mu_+\frac{\Lambda_{\rm PDS} - \gamma_+}{\Lambda_{\rm PDS} - \gamma_0}\right), \tag{C7}$$

$$\begin{aligned}\beta_4 = \Bigg[&\frac{1}{\pi}C_2^{(+)}\mu_0(-2\gamma_0^2)(\Lambda_{\rm PDS} - \gamma_0) - \frac{1}{\pi}C_2^{(-)}\mu_+(-\gamma_0^2 - \gamma_+^2)(\Lambda_{\rm PDS} - \gamma_+)\\ &+ 2\pi\left(\frac{\mu_0^2}{\gamma_0} + \frac{\mu_+^2}{\gamma_+}\right)^{-1}\Bigg[-\frac{1}{\pi^2}C_2^{(+)}\mu_+^3(\gamma_+ - \Lambda_{\rm PDS})(2\gamma_+ - \Lambda_{\rm PDS}) - \frac{1}{\pi^2}C_2^{(+)}\mu_0^3(\gamma_0 - \Lambda_{\rm PDS})(2\gamma_0 - \Lambda_{\rm PDS})\\ &- \frac{C_2^{(-)}(\gamma_+^2 + \gamma_0^2)\mu_+\mu_0}{2\pi}\left(\frac{\mu_+}{\gamma_0}(\Lambda_{\rm PDS} - \gamma_0) + \frac{\mu_0}{\gamma_+}(\Lambda_{\rm PDS} - \gamma_+)\right) + \frac{C_2^{(-)}\mu_+\mu_0(\mu_+ + \mu_0)}{\pi^2}(\Lambda_{\rm PDS} - \gamma_+)(\Lambda_{\rm PDS} - \gamma_0)\Bigg]\Bigg],\end{aligned} \tag{C8}$$

$$\beta_5 = \frac{1}{\pi}C_2^{(+)}\mu_0(\Lambda_{\rm PDS} - \gamma_0) - \frac{1}{\pi}C_2^{(-)}\mu_+(\Lambda_{\rm PDS} - \gamma_+) + \frac{B_1^{(3)}f_\pi}{4\pi g}(\gamma_0 - \Lambda_{\rm PDS}) - \frac{B_1^{(4)}f_\pi}{4\pi g}(\gamma_+ - \Lambda_{\rm PDS})\frac{\mu_+}{\mu_0}. \tag{C9}$$

It is instructive to take the isospin limit of these β expressions and compare to XEFT. Referring to Eq. (6), we can write down the B_1 couplings in this limit:

$$B_1^{(1)} = -B_1^{(2)} = -\sqrt{2}B_1^{(I=0)},$$
$$B_1^{(3)} = 2(B_1^{(I=1)} + B_1^{(I=0)}),$$
$$B_1^{(4)} = 2(B_1^{(I=1)} - B_1^{(I=0)}). \tag{C10}$$

Then, taking $\mu_+ = \mu_0 = \mu$, $\gamma_+ = \gamma_0 = \gamma$, we find

$$\beta_1 = \beta_3 = \beta_5 = \frac{1}{\pi}(\gamma - \Lambda_{\rm PDS})\left(\frac{B_1^{(I=0)}f_\pi}{g} - 2C_2^{(0)}\mu\right),$$
$$\beta_2 = \beta_4 = -\frac{4C_2^{(0)}\mu\gamma}{\pi}(\gamma - \Lambda_{\rm PDS})^2. \tag{C11}$$

The isospin-1 couplings drop out, which is to be expected, given that we have projected out the isospin-0 state and are here dropping isospin-breaking interactions. These expressions also match the dependence of the decay rate on C_2 and B_1 in XEFT [27]. Using Eq. (24) of Ref. [27] (and adjusting for a factor of 4 in the definition of C_2 in that paper), we see that $\beta_2 = \beta_4 = -\gamma r_0$ in the isospin limit. It is an important check on our calculation that in the isospin limit, the theory can be properly renormalized with isospin-respecting counterterms. When isospin breaking in the masses and binding momentum is included, isospin breaking in the B_1 operators needs to be included, as we have done in this paper.

[1] F. Muheim, *The European Physical Society Conference on High Energy Physics* (2021), https://indico.desy.de/event/28202/contributions/102717/.
[2] I. Polyakov, *The European Physical Society Conference on High Energy Physics* (2021), https://indico.desy.de/event/28202/contributions/105627/.
[3] L. An, *19th International Conference on Hadron Spectroscopy and Structure* (2021), https://indico.nucleares.unam.mx/event/1541/session/4/contribution/35/material/slides/0.pdf.
[4] R. Aaij *et al.* (LHCb Collaboration), Nat. Phys. **18**, 751 (2022).
[5] R. Aaij *et al.* (LHCb Collaboration), Nat. Commun. **13**, 3351 (2022).
[6] S. Fleming, R. Hodges, and T. Mehen, Phys. Rev. D **104**, 116010 (2021).
[7] L. Meng, G.-J. Wang, B. Wang, and S.-L. Zhu, Phys. Rev. D **104**, 051502 (2021).
[8] S. S. Agaev, K. Azizi, and H. Sundu, Nucl. Phys. **B975**, 115650 (2022).
[9] T.-W. Wu, Y.-W. Pan, M.-Z. Liu, S.-Q. Luo, X. Liu, and L.-S. Geng, Phys. Rev. D **105**, L031505 (2022).
[10] X.-Z. Ling, M.-Z. Liu, L.-S. Geng, E. Wang, and J.-J. Xie, Phys. Lett. B **826**, 136897 (2022).
[11] R. Chen, Q. Huang, X. Liu, and S.-L. Zhu, Phys. Rev. D **104**, 114042 (2021).
[12] X.-K. Dong, F.-K. Guo, and B.-S. Zou, Commun. Theor. Phys. **73**, 125201 (2021).
[13] A. Feijoo, W. H. Liang, and E. Oset, Phys. Rev. D **104**, 114015 (2021).
[14] M.-J. Yan and M. P. Valderrama, Phys. Rev. D **105**, 014007 (2022).
[15] L.-Y. Dai, X. Sun, X.-W. Kang, A. P. Szczepaniak, and J.-S. Yu, Phys. Rev. D **105**, L051507 (2022).
[16] X.-Z. Weng, W.-Z. Deng, and S.-L. Zhu, Chin. Phys. C **46**, 013102 (2022).
[17] Y. Huang, H. Q. Zhu, L.-S. Geng, and R. Wang, Phys. Rev. D **104**, 116008 (2021).
[18] R. Chen, N. Li, Z.-F. Sun, X. Liu, and S.-L. Zhu, Phys. Lett. B **822**, 136693 (2021).
[19] Q. Xin and Z.-G. Wang, Eur. Phys. J. A **58**, 110 (2022).
[20] M. Albaladejo, Phys. Lett. B **829**, 137052 (2022).
[21] M.-L. Du, V. Baru, X.-K. Dong, A. Filin, F.-K. Guo, C. Hanhart, A. Nefediev, J. Nieves, and Q. Wang, Phys. Rev. D **105**, 014024 (2022).
[22] Y. Jin, S.-Y. Li, Y.-R. Liu, Q. Qin, Z.-G. Si, and F.-S. Yu, Phys. Rev. D **104**, 114009 (2021).
[23] L. M. Abreu, F. S. Navarra, M. Nielsen, and H. P. L. Vieira, Eur. Phys. J. C **82**, 296 (2022).
[24] L. R. Dai, R. Molina, and E. Oset, Phys. Rev. D **105**, 016029 (2022).
[25] C. Deng and S.-L. Zhu, Phys. Rev. D **105**, 054015 (2022).
[26] K. Azizi and U. Özdem, Phys. Rev. D **104**, 114002 (2021).
[27] S. Fleming, M. Kusunoki, T. Mehen, and U. van Kolck, Phys. Rev. D **76**, 034006 (2007).
[28] S. Fleming and T. Mehen, Phys. Rev. D **78**, 094019 (2008).
[29] S. Fleming and T. Mehen, Phys. Rev. D **85**, 014016 (2012).
[30] T. Mehen and R. Springer, Phys. Rev. D **83**, 094009 (2011).
[31] A. Margaryan and R. P. Springer, Phys. Rev. D **88**, 014017 (2013).
[32] E. Braaten, H.-W. Hammer, and T. Mehen, Phys. Rev. D **82**, 034018 (2010).
[33] D. L. Canham, H.-W. Hammer, and R. P. Springer, Phys. Rev. D **80**, 014009 (2009).
[34] M. Jansen, H.-W. Hammer, and Y. Jia, Phys. Rev. D **89**, 014033 (2014).
[35] M. Jansen, H.-W. Hammer, and Y. Jia, Phys. Rev. D **92**, 114031 (2015).
[36] T. Mehen, Phys. Rev. D **92**, 034019 (2015).
[37] M. H. Alhakami and M. C. Birse, Phys. Rev. D **91**, 054019 (2015).
[38] E. Braaten, Phys. Rev. D **91**, 114007 (2015).
[39] E. Braaten, L.-P. He, K. Ingles, and J. Jiang, Phys. Rev. D **101**, 096020 (2020).
[40] E. Braaten, L.-P. He, and J. Jiang, Phys. Rev. D **103**, 036014 (2021).
[41] E. Braaten, L.-P. He, K. Ingles, and J. Jiang, Phys. Rev. D **103**, L071901 (2021).
[42] F.-K. Guo, C. Hidalgo-Duque, J. Nieves, A. Ozpineci, and M. P. Valderrama, Eur. Phys. J. C **74**, 2885 (2014).
[43] L. Dai, F.-K. Guo, and T. Mehen, Phys. Rev. D **101**, 054024 (2020).
[44] M. B. Wise, Phys. Rev. D **45**, R2188 (1992).
[45] G. Burdman and J. F. Donoghue, Phys. Lett. B **280**, 287 (1992).
[46] T.-M. Yan, H.-Y. Cheng, C.-Y. Cheung, G.-L. Lin, Y. C. Lin, and H.-L. Yu, Phys. Rev. D **46**, 1148 (1992); **55**, 5851(E) (1997).
[47] F.-K. Guo, C. Hanhart, U.-G. Meißner, Q. Wang, Q. Zhao, and B.-S. Zou, Rev. Mod. Phys. **90**, 015004 (2018).
[48] D. B. Kaplan, M. J. Savage, and M. B. Wise, Phys. Rev. C **59**, 617 (1999).
[49] D. B. Kaplan, M. J. Savage, and M. B. Wise, Phys. Lett. B **424**, 390 (1998).
[50] E. Braaten and A. Nieto, Phys. Rev. D **51**, 6990 (1995).
[51] L. Liu, K. Orginos, F.-K. Guo, C. Hanhart, and U.-G. Meissner, Phys. Rev. D **87**, 014508 (2013).